J Mol Model (2014) 20:2517
DOI 10.1007/s00894-014-2517-9

ORIGINAL PAPER

An electro-optical and electron injection study of benzothiazole-based squaraine dyes as efficient dye-sensitized solar cell materials: a first principles study

Najat Saeed AL-Fahdan · Abdullah M. Asiri · Ahmad Irfan · Salem A. Basaif · Reda M. El-Shishtawy

Received: 22 July 2014 / Accepted: 31 October 2014 / Published online: 25 November 2014

Abstract Squaraine dyes have attracted significant attention in many areas of daily life from biomedical imaging to semiconducting materials. Moreover, these dyes are used as photoactive materials in the field of solar cells. In the present study, we investigated the structural, electronic, photophysical, and charge transport properties of six benzothiazole-based squaraine dyes (Cis-SQ1–Cis-SQ3 and Trans-SQ1–Trans-SQ3). The effect of electron donating ($-OCH_3$) and electron withdrawing (−COOH) groups was investigated intensively. Ground state geometry and frequency calculations were performed by applying density functional theory (DFT) at B3LYP/6-31G** level of theory. Absorption spectra were computed in chloroform at the time-dependent DFT/B3LYP/6-31G** level of theory. The driving force of electron injection (ΔG^{inject}), relative driving force of electron injection (ΔG_r^{inject}), electronic coupling constants ($|V_{RP}|$) and light harvesting efficiency (LHE) of all six compounds were calculated and compared with previously studied sensitizers. The ΔG^{inject}, ΔG_r^{inject} and $|V_{RP}|$ of all six compounds revealed that these sensitizers would be efficient dye-sensitized solar cell materials. Cis/Trans-SQ3 exhibited superior LHE as compared to other derivatives. The Cis/Trans geometric effect was studied and discussed with regard to electro-optical and charge transport properties.

N. S. AL-Fahdan · A. M. Asiri · S. A. Basaif · R. M. El-Shishtawy
Chemistry Department, Faculty of Science, King Abdulaziz University, PO Box 80203, Jeddah 21589, Saudi Arabia

A. M. Asiri
Center of Excellence for Advanced Materials Research, King Abdulaziz University, PO Box 80203, Jeddah 21589, Saudi Arabia

A. Irfan (✉)
Department of Chemistry, Faculty of Science, King Khalid University, Abha 61413PO Box 9004, Saudi Arabia
e-mail: irfaahmad@gmail.com

Keywords Renewable energy · Photovoltaic · Ab initio calculations · Electronic properties · Charge transport properties · Electron injection

Introduction

To develop renewable, low cost, environmental friendly and sustainable energy is the major energy issue of the current era [1]. Organic materials have attracted significant attention in this regard as they are cheap, pollution free, easy to modify chemically, and have structural flexibility [2–6]. The squaraine dyes are efficient organic materials that are used for multifunctional purposes, e.g., in bioimaging applications [7], sensors [8] and semiconducting devices such as laser technology [9], organic light emitting diodes (OLEDs) [10], organic field effect transistors (OFETs), and photovoltaic cells [11–13]. Additionally, thiophene-based materials are promising because of their semiconducting nature [14], non-linear optical behavior [15] and efficient electron transport properties [16]. Squaraine dyes are used as dye-sensitized solar cells (DSSCs) [17], organic solar cells [18], organic–inorganic hybrid solar cells [19], etc. In previous studies, the electronic/charge transport properties and efficiency of DSSCs have been developed by incorporating thiophene, pyrrole and thiazole unit(s) into squaraine dyes [17, 20, 21]. Bridge elongation, introduction of electron-withdrawing groups and/or push-pull strategies are good approaches to enhance the efficiency, intra-molecular charge transfer (ICT) and stability of sensitizers [22–27]. Larger light harvesting ability, ICT and electronic coupling constants [light harvesting efficiencies (LHE)] would lead to more efficient DSSCs. Dye aggregation and charge recombination generally leads to lower efficiency [28–31].

In the present study, we selected for study 2-3-(2-ethoxy-2-oxoethyl) benzo [d] thiazol-2 (3H)-ylidene) methyl)-4-((3-(2-

ethoxy-2-oxoethyl) benzo [d] thiazol-3-ium-2-yl) methylene)-3-oxocyclobut-1-enolate (Cis-SQ1) and two of its derivatives (Cis-SQ2 and Cis-SQ3). In Cis-SQ2 and Cis-SQ3, –COOH and –OCH3 groups have been substituted at each end of the benzo[d]thiazol core. Moreover, three more benzothiazole-based squaraine dyes were designed: Trans-SQ1–Trans-SQ3 (Fig. 1). All six sensitizers have long side chains and acidic ligands, with the expectation that this might inhibit recombination and diminish aggregation, resulting in improved DSSC efficiency. The investigations were carried out with the aim of shedding some light on the structural/electro-optical properties, driving force of electron injection ($\Delta G^{inject.}$), relative values of the driving force of electron injection ($\Delta G_r^{inject.}$), electronic coupling constants ($|V_{RP}|$) and LHE. Finally, we shed light on factors affecting the short-circuit current density (J_{sc}) and open-circuit voltage (V_{oc}), and conclude with a discussion on the nature of sensitizers.

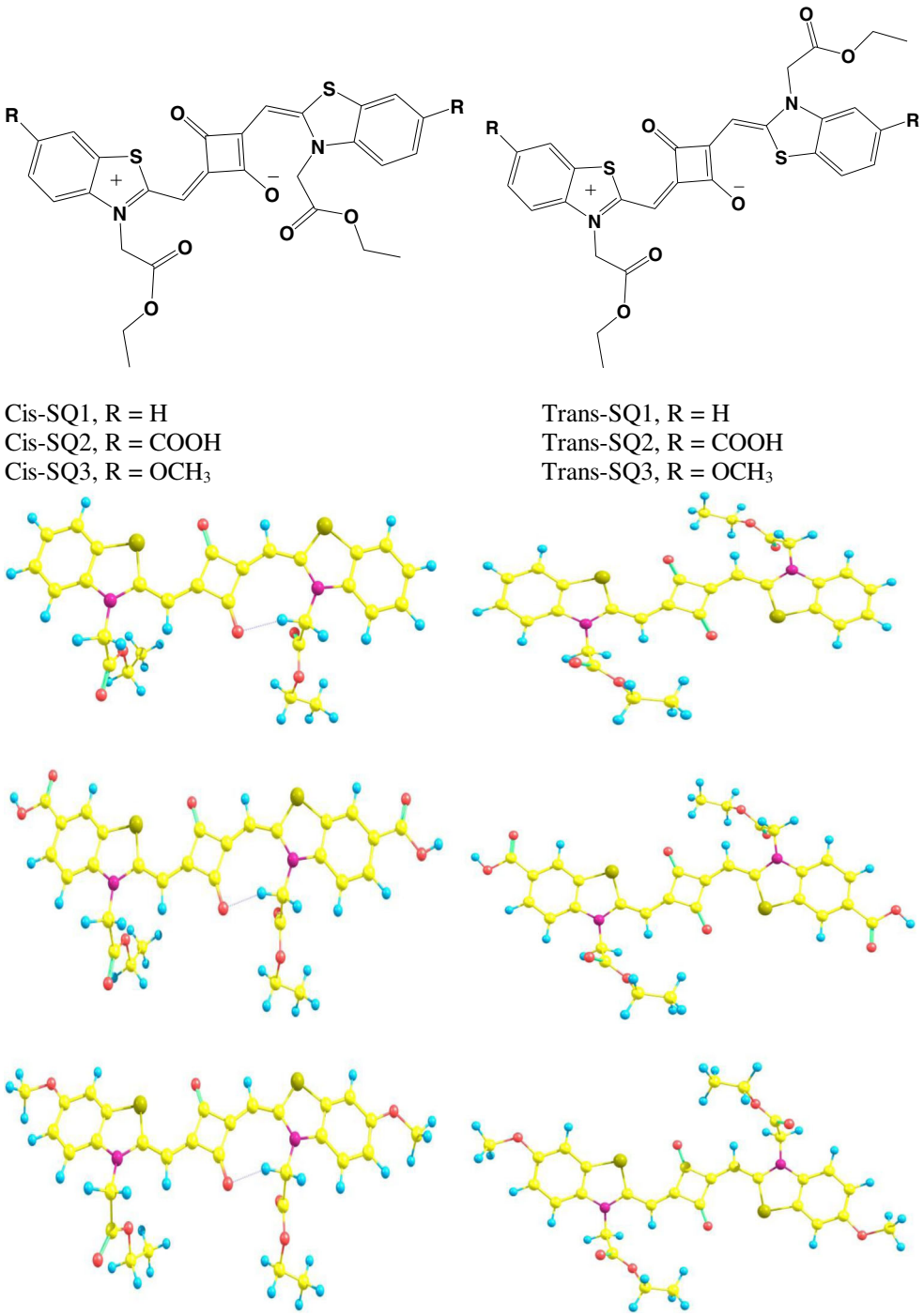

Fig. 1 The structures of the squaraine dyes (*left* Cis, *right* Trans) investigated in the present study. *Top panel* Schematic, *bottom panel* optimized structures

The $\Delta G_r^{inject.}$ and $|V_{RP}|$ of these six benzothiazole-based squaraine dyes were compared with the recently synthesized dyenitro sensitizer, which has calculated values of −0.39 and 0.195, respectively [25]. The $\Delta G_r^{inject.}$ and $|V_{RP}|$ values were also compared with those of some other previously studied sensitizers. The present study has yielded interesting results that will have an impact in this field and motivate experimentalists. To the best of our knowledge, no computational study has been carried out previously on these squaraine dyes. For the first time, we investigate interesting properties of these squaraine dyes with respect to DSSCs. The paper is structured as follows: Computational details presents an outline of density functional theory (DFT) and time-dependent DFT (TDDFT), including the rationale for choosing the hybrid functional and the basis set; the Results and discussion section presents the structural, electronic, optical and charge transport properties of DSSCs; the major conclusions of the present investigations are summarized in Conclusions.

Computational details

Density functional theory is good approach that reproduces experimental evidence for small organic molecules; among different functionals, B3LYP provides the best depiction [32–39]. The absorption spectra of hydrazone, azobenzene, anthraquinone, phenylamine and indigo dyes have been calculated previously by applying B3LYP functional with an average deviation=0.20 eV [40]. In our previous studies, we pointed out that the B3LYP and TD-B3LYP are reasonable choices that reproduce experimental, as well as already computed, structural, electro-optical and electron injection properties [25, 41, 42] of azo dyes [43, 44], triphenylamine dyes [26], chemosensors [45], phthalocyanines [24], biologically active molecules [46], and oxadiazoles [47]. More recently, the experimental electronic and charge transport properties of thiophene-based materials have been reproduced by applying the B3LYP/6-31G** level of theory [38]. Preat and coworkers [28, 48] studied the electron injection of some organic compounds and concluded that the B3LYP/6-31G** level of theory is adequate. Huong et al. [49] optimized the geometries of naphtho [2,3-*b*] thiophene at two different levels of theories, i.e., B3LYP/6-31G** and PBE0/6-31G** and found that the electronic as well as charge transport properties calculated at B3LYP/6-31G** level of theory are in good agreement with experimental results. TDDFT has also proved an efficient approach that can reproduce experimental absorption and emission spectra [50]. Thus, in the present study, ground state geometries and electronic properties were computed at DFT/B3LYP/6-31G** and absorption spectra at TD-B3LYP/6-31G** levels of theories. Excitation energies were calculated in chloroform using the polarizable continuum model (PCM).

The rate of the electron/charge transfer process from dye to metal oxides can be explained by Marcus theory according to Eq. 1 [51–56]:

$$k_{inject.} = \cdot|V_{RP}\cdot|2/h\cdot\left(\pi\Big/\lambda k_B T\right)^{1/2\cdot}\exp\left[\cdot\text{–}\cdot\ \Delta G^{inject.}\text{–}\cdot\lambda\right)^2/4\lambda k_B T\Big] \quad (1)$$

In Eq. 1, k_{inject} is the rate constant (in S^{-1}) of the electron injection from dye to TiO_2, k_BT is the Boltzmann constant, h is Planck's constant, ΔG^{inject} the driving force of electron injection, λ is the reorganization energy and $|V_{RP}|$ is the electronic coupling constant. It can be seen from Eq. 1 that superior $|V_{RP}|$ would increase the rate constant, resulting in a more efficient sensitizer. The $|V_{RP}|$ for a photoinduced charge transfer can be calculated by generalized Mulliken-Hush formalism [52, 53]. Hsu et al. [53] stated that $|V_{RP}|$ can be evaluated by half of the injection driving force (ΔE_{RP}) as:

$$|V_{RP}| = \Delta E_{RP}/2 \quad (2)$$

Here, ΔE_{RP} can be expressed within Koopman's approximation as:

$$\Delta E_{RP} = \left[E_{LUMO}^{dye} + 2E_{HOMO}^{dye}\right] - \left[E_{LUMO}^{dye} + E_{HOMO}^{dye} + E_{CB}^{TiO_2}\right] \quad (3)$$

Where E_{LUMO}^{dye} and E_{HOMO}^{dye} correspond to the lowest unoccupied molecular orbital (LUMO) and highest occupied molecular orbital (HOMO) of the dye, respectively. The conduction band edge of TiO_2 ($E_{CB}^{TiO_2}$) is difficult to determine accurately due to its sensitive dependence on the conditions, e.g., the pH of the solution. Thus we used an experimental value corresponding to conditions where the semiconductor is in contact with aqueous redox electrolytes fixed at pH 7.0, i.e., $E_{CB}^{TiO_2} = -4.0$ eV [57–59]. The E_{LUMO}^{dye} also corresponds to the reduction potential of the dye (E_{RED}^{dye}) while the E_{HOMO}^{dye} is related to the potential of first oxidation (i.e., $-E_{HOMO}^{dye} = E_{OX}^{dye}$) thus Eq. (3) can be expressed as:

$$\Delta E_{RP} = \left[E_{HOMO}^{dye} - E_{CB}^{TiO_2}\right] = -\left[E_{OX}^{dye} + E_{CB}^{TiO_2}\right] \quad (4)$$

Equation (4) can be rewritten as:

$$\Delta E_{RP} = E_{0-0}^{dye} - \left[2E_{OX}^{dye} + E_{RED}^{dye} + E_{CB}^{TiO_2}\right] \quad (5)$$

To evaluate the oxidation potential of excited dye, and to calculate the electron injection onto the TiO_2 surface, we shed light on the free energy change (in eV) which can be expressed as [58]:

$$\Delta G^{inject} = E_{OX}^{dye*} - E_{CB}^{TiO_2} \quad (6)$$

where E_{OX}^{dye*} is the oxidation potential of the dye in the excited state. Two models can be used to estimate E_{OX}^{dye*} [60, 61]. The

first states that electron injection occurs from the unrelaxed excited state. The excited state oxidation potential can then be extracted from the redox potential of the ground state, E_{OX}^{dye} and the vertical transition energy corresponding to the photo-induced ICT,

$$E_{OX}^{dye*} = E_{OX}^{dye} - \lambda_{\max}^{ICT} \quad (7)$$

where λ_{max}^{ICT} is the energy of the ICT. Note that this relation is valid only if the entropy change during the light absorption process can be neglected. Preat and co-authors [28, 48, 62] showed that λ_{max}^{ICT} can be evaluated during the electronic excitation, which is equal to the absorption energy. Thus, in the present study, we evaluated λ_{max}^{ICT} from the absorption energies of the specific excitation.

For the second model, it is assumed that electron injection occurs after relaxation. Given this condition, E_{OX}^{dye*} is expressed as [61]:

$$E_{OX}^{dye*} = E_{OX}^{dye} - E_{0-0}^{dye} \quad (8)$$

where E_{0-0}^{dye} is the transition energy between the ground electronic state/ground vibrational state (n=0/v=0) and the first excited electronic state/ground vibrational state (n=1/v=0). This is denoted as 0–0 and is defined as the "lowest energy transition". To estimate the 0–0 "absorption" line, both S_0 (singlet ground state) and S_1 (first singlet excited state) equilibrium geometries, Q_{S0} and Q_{S1}, respectively, are required. Electron injection has been observed previously from unrelaxed excited states in TiO_2 [63] and SnO_2 [64]. Most experimentalists assume that electron injection ensues after relaxation but the relative contribution of an ultrafast injection path is not clear. Preat et al. [48] pointed out that the absolute difference between the relaxed and unrelaxed ΔG_{inject} is constant, and is of the same order of magnitude as that of the E_{OX}^{dye} and E_{OX}^{dye*} mean average error. The ΔG^{inject} and E_{OX}^{dye*} were evaluated using Eqs. (6) and (7).

The LHE of the dye has to be as high as possible to maximize the photocurrent response. The LHE can be expressed as [65]:

$$\mathrm{LHE} = 1 - 10^{-A} = 1 - 10^{-f} \quad (9)$$

where $A(f)$ is the absorption (oscillator strength) of the dye associated with λ_{max}^{ICT}. The oscillator strength is derived directly from TDDFT calculations as follows:

$$f = \frac{2}{3}\lambda_{\max}^{ICT}\left|\overrightarrow{\mu}\mathrm{o{-}ICT}\right|^2 \quad (10)$$

where μo−ICT is the dipolar transition moment associated with the electronic excitation. In order to maximize f, both λ_{max}^{ICT} and μo−ICT must be large [66, 67].

The efficiency (η) of solar cells can be determined using the following equation:

$$\eta = FF\frac{V_{oc}J_{sc}}{P_{inc}} \quad (11)$$

where J_{sc} is the short-circuit current density, V_{oc} the open circuit voltage, FF the fill factor, and P_{inc} the intensity of the incident light. The J_{sc} can be evaluated as

$$J_{sc} = \int_{\lambda} LHE(\lambda)\phi_{injection}\eta_{collection}d\lambda \quad (12)$$

where $\eta_{collection}$ is the charge collection efficiency, which is constant. From above equation, we can find that J_{sc} is linked directly with the LHE and $\phi_{injection}$ is electron injection efficiency, which is related to ΔG^{inject}. It is revealing that higher LHE and ΔG^{inject} would lead to efficient devices [68].

Results and discussion

Geometries

Selected bond lengths and bond angles of six benzothiazole-based squaraine sensitizers (both Cis and Trans) are listed in Table 1. All the selected geometrical parameters of Cis and Trans sensitizers are very similar, revealing that changing the geometry from Cis to Trans forms has no significant effect on bond distances/bond angles. In both Cis/Trans-SQ2, the C_1–N_1 bond lengths shortened while Cis/Trans-SQ3 was lengthened compared to Cis/Trans-SQ1. In Cis/Trans-SQ2, the C_3–N_1 bond lengths lengthened while in Cis/Trans-SQ3 they shortened compared to Cis/Trans-SQ1. In Cis/Trans-SQ3, C_3–S_1 was lengthened compared to this bond in Cis/Trans-SQ1. The C_1–N_1 bond is adjacent to, while the C_3–N_1 bond is distant from, the electron withdrawing (−COOH) and donating (–OCH_3) groups. Thus, it was thought that lengthening of C_3–N_1 in Cis/Trans-SQ2 is due to the withdrawing effect of –COOH, which withdraws the electron charge density towards itself. The shortening of C_3–N_1 in Cis/Trans-SQ3 is due to the donating effect of –OCH_3, which donates electrons. The electron charge density withdrawing/donating by electron withdrawing/electron donating groups results in lengthening/shortening of bond lengths in good agreement with previous studies [69].

Frontier molecular orbitals and absorption spectra

The charge density distribution patterns of the ground state frontier molecular orbitals, HOMOs (and HOMOs−1), and LUMOs (and LUMOs+1) of the six Cis/Trans-SQ1-SQ3 benzothiazole-based squaraine sensitizers are illustrated in Fig. 2. In all the studied compounds, the HOMOs−1 are

Table 1 Geometrical parameters, bond lengths (Å) and bond angles (°) of benzothiazole-based squaraine dyes optimized at B3LYP/6-31G** level of theory

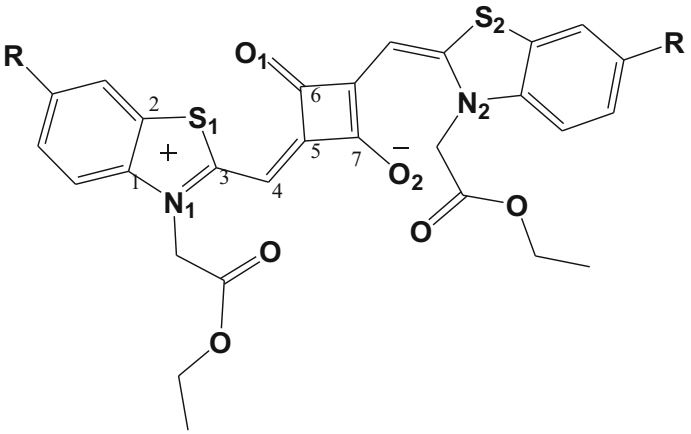

	Cis-SQ1	Cis-SQ2	Cis-SQ3	Trans-SQ1	Trans-SQ2	Trans-SQ3
			Bond lengths			
C_1-C_2	1.404	1.407	1.405	1.405	1.408	1.407
C_1-N_1	1.397	1.391	1.400	1.398	1.391	1.400
C_3-N_1	1.383	1.387	1.381	1.382	1.386	1.380
C_3-S_1	1.770	1.769	1.773	1.765	1.765	1.768
C_2-S_1	1.765	1.765	1.765	1.766	1.766	1.766
C_6-O_1	1.228	1.227	1.228	1.233	1.232	1.233
C_7-O_2	1.236	1.236	1.237	1.233	1.232	1.233
			Bond angles			
C_1-N_1-C_3	115.20	115.19	115.21	115.21	115.21	115.19
N_1-C_3-S_1	110.35	110.42	110.32	110.59	110.65	110.62
S_1-C_3-C_4	125.34	125.51	125.22	126.04	126.19	125.92
C_3-C_4-C_5	127.03	126.96	127.17	127.74	127.58	127.85
C_5-C_6-O_1	136.60	136.59	136.55	136.19	136.17	136.18
C_5-C_7-O_2	133.18	133.22	133.16	134.42	134.51	134.40

localized on the squaraine moiety. The charge densities of HOMOs and LUMOs are distributed throughout the backbone. The LUMOs+1 are localized on benzothiazole moieties in all the studied squaraine sensitizers. In Cis/Trans-SQ2, the electron-withdrawing group is –COOH, while in other sensitizers, the carbonyl group of 2-3-(2-ethoxy-2-oxoethyl) units also take part in the formation of LUMOs and LUMOs+1. In the LUMOs and LUMOs+1 of Trans-SQ1–Q3, the charge density distribution on 2-3-(2-ethoxy-2-oxoethyl) moieties is less than that on Cis-SQ1–SQ3.

The calculated energies of HOMO (E_{HOMOs}), LUMO (E_{LUMOs}), and LUMOs+1 ($E_{LUMOs+1}$), and the energy gaps (E_g) of the six Cis/Trans-SQ1–SQ3 benzothiazole-based squaraine sensitizers at B3LYP/6-31G** level of theory are tabulated in Table 2. The –COOH groups lower the energies of E_{HOMOs}, E_{LUMOs} and $E_{LUMOs+1}$ while $–OCH_3$ boosts them up. The smallest E_g values were observed for Cis/Trans-SQ2, which has –COOH groups at the –R positions. The computed E_g of all the six sensitizers are smaller than that of the dyenitro, i.e., 2.81 eV [23] suggesting that DSSC efficiency might be improved in the former compounds. The smaller E_{LUMOs} of Cis/Trans-SQ2 reveal that the injected electrons would be more stable, and that the charge transport cannot be quenched by losing electrons.

The acidic ligands in Cis/Trans-SQ2 are good light-harvesting portions that help anchor the sensitizer to the TiO_2 surface. They also enhance solubility in solution and diminish aggregation [70]. From the charge density distribution on LUMOs (see Fig. 2), it is expected that the Cis/Trans-SQ2 would be more stable after anchoring with the TiO_2 surface. Moreover, –COOH would be a favorable site from which to transfer electrons from dyes to the TiO_2 surface. Furthermore, side chains might create a barrier between holes in the redox couple and electrons in the TiO_2 to inhibit recombination.

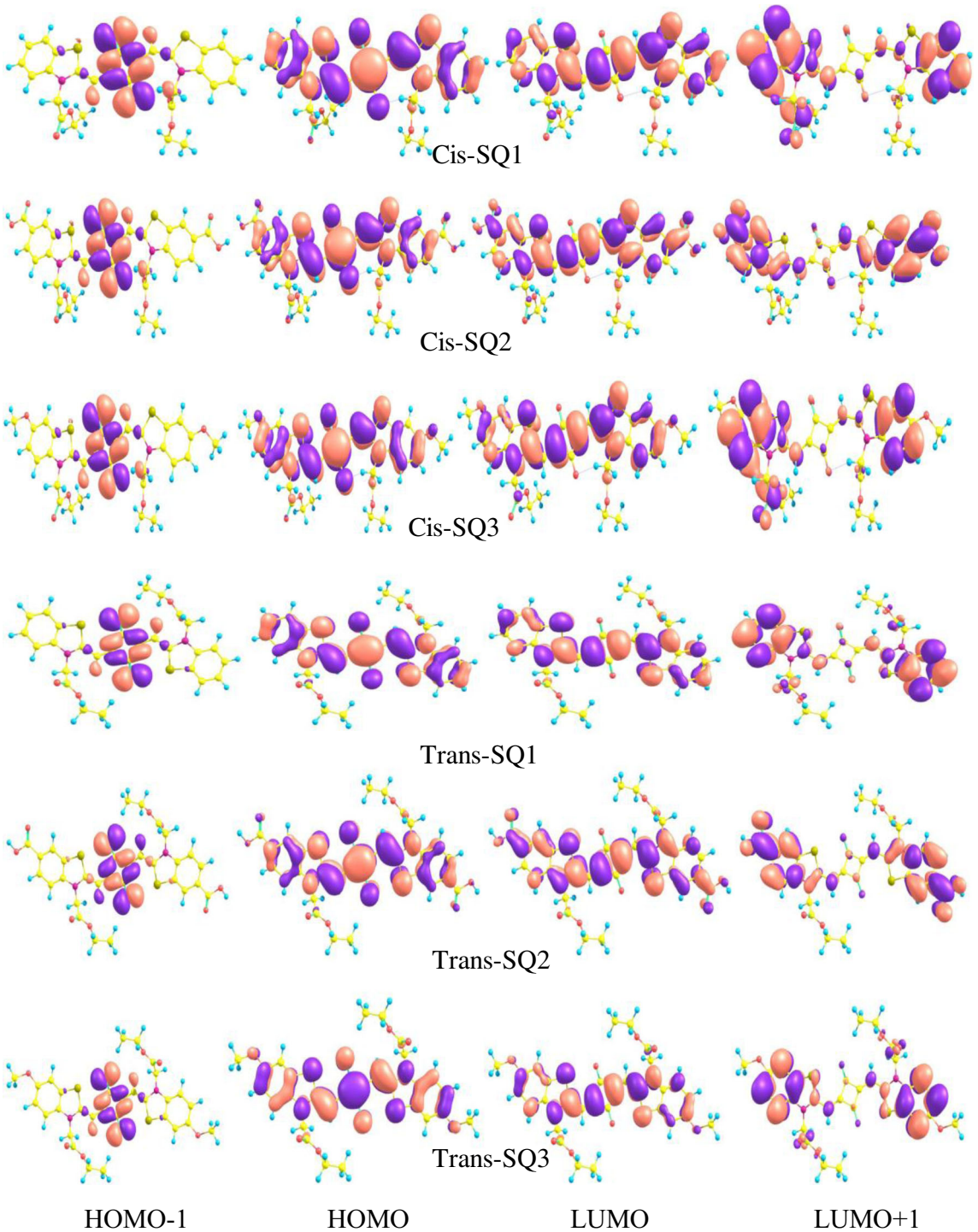

Fig. 2 Charge density distribution of the frontier molecular orbitals (0.02 contour value) of the studied systems at B3LYP/6-31G** level of theory

In our previous study, we shed light on the charge transport behavior with respect to the size of the TiO_2 and found that the ICT from dye to TiO_2 nanoparticles improved by increasing the size of the TiO_2 crystal [71]. The inorganic materials, e.g., TiO_2, in the photovoltaic devices would overwhelm the photo-induced degradation of the dyes. Moreover, the photogeneration of charge transporters would lead to excitons being absorbed by the TiO_2 [72, 73]. Additionally, absorption yield can be enhanced by incorporating TiO_2 [74].

The calculated absorption wavelengths (λ_a), oscillator strengths (*f*) and major transitions of benzothiazole-based squaraine dyes at TD-B3LYP/6-31G** level of theory in

Table 2 Calculated highest occupied molecular orbital energies (E_{HOMO}), lowest unoccupied molecular orbital energies (E_{LUMO}), LUMO+1 energies (E_{LUMO+1}), energy gaps (E_g) and absorption wavelengths (λ_a) of benzothiazole-based squaraine dyes (in chloroform) at B3LYP/6-31G** and TD-B3LYP/6-31G** level of theories

Compounds	E_{HOMO} (eV)	E_{LUMO} (eV)	E_{LUMO+1} (eV)	E_g (eV)	λ_a (nm)[a]	f[b]	Transition
Cis-SQ1	−4.43	−2.28	−0.60	2.15	630	1.796	H ->L
Cis-SQ2	−4.72	−2.64	−1.52	2.08	655	1.911	H ->L
Cis-SQ3	−4.29	−2.15	−0.58	2.14	638	1.950	H ->L
Trans-SQ1	−4.41	−2.26	−0.51	2.15	639	1.623	H ->L
Trans-SQ2	−4.68	−2.60	−1.45	2.08	664	1.715	H ->L
Trans-SQ3	−4.26	−2.12	−0.49	2.14	648	1.766	H ->L

[a] Experimental λ_a in chloroform = 671 nm

[b] Oscillator strength

chloroform are tabulated in Table 2. The computed λ_a of Cis-SQ1 upon the transition from H ->L was observed to be 630 nm, which is in good agreement with the experimentally measured value of 671 nm. The calculated λ_a of Cis-SQ2, Cis-SQ3, Trans-SQ1–Trans-SQ3 are red shifted by 25, 8, 9, 34 and 18 nm compared to Cis-SQ1. Trans-SQ1–SQ3 are red shifted more than Cis-SQ1–SQ3.

Short-circuit current density

The ΔG^{inject}, E_{OX}^{dye}, E_{OX}^{dye*}, λ_{max}^{ICT}, LHE, $|V_{RP}|$ and ΔG_r^{inject} of the six benzothiazole-based squaraine dyes are presented in Table 3. The negative computed values of ΔG^{inject} mean that the excited state of the dye lies above the conduction band edge of TiO_2, which would favor electron injection from the dye's excited state to the conduction band edge of TiO_2. From Eq. 12 it can be found that the improvement of the short-circuit current density, J_{sc}, is related directly to the LHE and Φ_{inject}. To maximize the photocurrent response, the LHE of the dyes must be improved. Additionally, there is another factor that can enhance J_{sc}, i.e., improvement of Φ_{inject}, which is related to ΔG^{inject}. Here, we first shed light on ΔG^{inject} then discuss the LHE. The ΔG^{inject} values of Cis-SQ1, Cis-SQ2, Cis-SQ3, Trans-SQ1, Trans-SQ2, and Trans-SQ3 are 3.37, 2.67, 3.54, 3.33, 2.64 and 3.54 times higher than that of the dyenitro compound. The Cis/Trans-SQ1 to -SQ3 sensitizers have superior $|V_{RP}|$ and ΔG^{inject} than the dyenitro. In all the studied sensitizers, the major transitions correspond to HOMO−>LUMO. The comparable $|V_{RP}|$ and ΔG_r^{inject} values for both Cis and Trans forms reveal that the change in geometry has no significant effect on improving electron injection. We observed that the –OCH_3 group at the terminal positions of benzothiazole is boosted up, while the –COOH group diminishes $|V_{RP}|$ and ΔG_r^{inject}.

The calculated ΔG^{inject} and $|V_{RP}|$ of all the benzothiazole-based squaraine sensitizers computed at TD-B3LYP/6-31G* level of theory were superior to all the hydrazone and azo dyes, i.e., dyenitro (−0.39 and 0.195 eV), 2-{4-[2-p-chlorobenzylidenehydrazino] phenyl}-ethylene-1,1,2-tricarbonitrile and 2-{4-[2-p-bromobenzylidenehydrazino] phenyl} ethylene-1,1,2-tricarbonitrile (−0.53 and 0.265 eV), respectively [43], and the azo dye 3-(4-methyl-phenylazo)-6-(4-nitro-phenylazo)-2,5,7-triaminopyrazolo [1,5-a] pyrimidine (−1.19 and 0.53 eV) [75], revealing improved electron injection in the set analyzed here.

Table 3 The ΔG^{inject}, ΔG_r^{inject}, oxidation potential, light harvesting efficiency (LHE), $|V_{RP}|$ of investigated dyes in chloroform at TD-B3LYP/6-31G** level of theory

System	ΔG^{inject} (eV)	E_{OX}^{dye} (eV)	E_{OX}^{dye*} (eV)	λ_{max}^{ICT} (eV)	f	LHE	ΔG_r^{inject} (eV)[a]	$\lvert V_{RP}\rvert$ (eV)
Dyenitro[b]	−0.39	5.96	3.61	2.35	1.319	0.9520	1.00	0.195
Cis-SQ1	−1.32	4.65	2.68	1.97	1.796	0.9840	3.37	0.660
Cis-SQ2	−1.04	4.86	2.96	1.90	1.911	0.9877	2.67	0.520
Cis-SQ3	−1.38	4.56	2.62	1.94	1.950	0.9888	3.54	0.690
Trans-SQ1	−1.30	4.64	2.70	1.94	1.623	0.9762	3.33	0.650
Trans-SQ2	−1.03	4.84	2.97	1.87	1.715	0.9807	2.64	0.515
Trans-SQ3	−1.38	4.53	2.62	1.91	1.766	0.9829	3.54	0.690

[a] ΔG_r^{inject} =relative electron injection ΔG^{inject} (dye)/ ΔG^{inject} (Dyenitro)

[b] Details can be found in reference [43]

The data in Table 3 reveal that the benzothiazole-based squaraine dyes have superior LHE compared to dyenitro. The Cis isomers have superior LHE compared to Trans isomers. The trend of LHE is as follows: Cis-SQ3>Cis-SQ2>Cis-SQ1>Trans-SQ3>Trans-SQ2>Trans-SQ1. The Cis/Trans-SQ3 have larger LHE followed by Cis/Trans-SQ2 as compared to the other studied systems.

The LHE and ΔG^{inject} values of the six benzothiazole-based squaraine sensitizers are superior to those of dyenitro (0.9520 and −0.39), 2-{4-[2-p-chlorobenzylidenehydrazino] phenyl}-ethylene-1,1,2-tricarbonitrile and 2-{4-[2-p-bromobenzylidenehydrazino] phenyl}-ethylene-1,1,2-tricarbonitrile (0.9208 and −0.53), respectively [43], and the azo dye 3-(4-methyl-phenylazo)-6-(4-nitro-phenylazo)-2,5,7-triaminopyrazolo [1,5-a] pyrimidine (0.8732 and −0.86) [75], revealing that the sensitizers studied in the present article would be efficient materials for DSSCs.

Open-circuit voltage

The relationship among the electronic structure of sensitizers and these quantities is unknown, thus the open-circuit voltage, V_{oc}, can be measured only experimentally. The energy relationship can be obtained according to the sensitized mechanism, single electron and single state approximation as under [76]:

$$eV_{oc} = E_{LUMO} - E_{CB} \quad (13)$$

It can be seen that, the greater the E_{LUMO} the larger the V_{oc}. In 2001, Brabec and co-workers [77] concluded that V_{oc} depends strongly on E_{LUMO}. The superior reduction potential (E_{LUMO}) of the Cis/Trans-SQ2 compared to the other sensitizers reveals that the V_{oc} of prior compounds would be larger than that of other counterparts. This is might be due to the –COOH groups, which are favorable sites from which to transfer electrons from dyes to the TiO_2 surface.

Conclusions

No significant effect on the structural properties, excitation energies, driving force of electron injection or electronic coupling constants was observed upon changing the geometry of benzothiazole-based squaraine dyes from Cis to Trans forms. Alterations in geometry usually decreases the LHE. The greater driving force of electron injection, electronic coupling constants, LHEs (short-circuit current densities) and V_{oc} of benzothiazole-based squaraine dyes compared to the corresponding values in the dyenitro, 2-{4-[2-p-chlorobenzylidenehydrazino] phenyl}-ethylene-1,1,2-tricarbonitrile, 2-{4-[2-p-bromobenzylidenehydrazino] phenyl} ethylene-1,1,2-tricarbonitrile and 3-(4-methyl-phenylazo)-6-(4-nitro-phenylazo)-2,5,7-triaminopyrazolo [1,5-a] pyrimidine showed that the squaraine sensitizers would be efficient DSSC materials. The improved LHEs and electron affinities (LUMO energies) of the Cis compared to the Trans isomer revealed that the former would be better sensitizers than the latter. We hope this work will be helpful in the design of organic dyes with targeted properties to improve the performance of dye-sensitized solar cells.

Acknowledgments This Project was funded by King Abdulaziz City for Science and Technology (KACST) through the National Science, Technology and Innovation Plan (NSTIP) under grant number 8-ENE198-3. The authors therefore acknowledge with thanks KACST for support for Scientific Research. Also, the authors are thankful to the Deanship of Scientific Research (DSR), King Abdulaziz University for technical support.

References

1. Goodenough JB Abruña HD, Buchanan MV (2007) Basic research needs for electrical energy storage. Report of the Basic Energy Sciences Workshop on Electrical Energy Storage. US Department of Energy/Basic Energy Sciences (DOE/BES), Washington DC. http://science.energy.gov/~/media/bes/pdf/reports/files/ees_rpt.pdf
2. Lan Y-K, Huang C-I (2008) J Phys Chem B 112:14857–14862. doi:10.1021/jp806967x
3. Weitz RT, Amsharov K, Zschieschang U et al (2008) J Am Chem Soc 130:4637–4645. doi:10.1021/ja074675e
4. Newman CR, Frisbie CD, da Silva Filho DA, Brédas J-L, Ewbank PC, Mann KR (2004) Chem Mater 16:4436–4451. doi:10.1021/cm049391x
5. Zaumseil J, Sirringhaus H (2007) Chem Rev 107:1296–1323. doi:10.1021/cr0501543
6. Chen H-Y, Chao I (2005) Chem Phys Lett 401:539–545. doi:10.1016/j.cplett.2004.11.125
7. Escobedo JO, Rusin O, Lim S, Strongin RM (2010) Curr Opin Chem Biol 14:64–70. doi:10.1016/j.cbpa.2009.10.022
8. Beverina L, Salice P (2010) Eur J Org Chem 2010:1207–1225. doi:10.1002/ejoc.200901297
9. Oswald B, Patsenker L, Duschl J, Szmacinski H, Wolfbeis OS, Terpetschnig E (1999) Bioconjugate Chem 10:925–931. doi:10.1021/bc9801023
10. Tatsuo Mori H-GK, Teruyoshi M, Duck-Chool L (2001) Jpn J Appl Phys 40:5346. doi:10.1143/JJAP.40.5346
11. Chen G, Sasabe H, Sasaki Y et al (2014) Chem Mater 26:1356–1364. doi:10.1021/cm4034929
12. Silvestri F, Irwin MD, Beverina L, Facchetti A, Pagani GA, Marks TJ (2008) J Am Chem Soc 130:17640–17641. doi:10.1021/ja8067879
13. Bagnis D, Beverina L, Huang H et al (2010) J Am Chem Soc 132:4074–4075. doi:10.1021/ja100520q
14. Irfan A, Cui R, Zhang J (2009) Theor Chem Acc 122:275–281. doi:10.1007/s00214-009-0506-3
15. Torruellas WE, Neher D, Zanoni R, Stegeman GI, Kajzar F, Leclerc M (1990) Chem Phys Lett 175:11–16. doi:10.1016/0009-2614(90)85510-J
16. Venkataraman L, Klare JE, Nuckolls C, Hybertsen MS, Steigerwald ML (2006) Nature 442:904–907. doi:10.1038/nature05037
17. Yen Y-S, Chou H-H, Chen Y-C, Hsu C-Y, Lin JT (2012) J Mater Chem 22:8734–8747. doi:10.1039/c2jm30362k

18. Fu Y-T, da Silva Filho DA, Sini G et al (2014) Adv Funct Mater 24: 3790–3798. doi:10.1002/adfm.201303941
19. Ruankham P, Macaraig L, Sagawa T, Nakazumi H, Yoshikawa S (2011) J Phys Chem C 115:23809–23816. doi:10.1021/jp204325y
20. Ooyama Y, Harima Y (2009) Eur J Org Chem 2009:2903–2934. doi: 10.1002/ejoc.200900236
21. Mishra A, Fischer MKR, Bäuerle P (2009) Angew Chem Int Ed 48: 2474–2499. doi:10.1002/anie.200804709
22. Al-Sehemi AG, Irfan A, Asiri AM, Ammar YA (2012) Spectrochim Acta A Mol Biomol Spectrosc 91:239–243
23. Al-Sehemi AG, Irfan A, Asiri AM, Ammar YA (2012) J Mol Struct 1019:130–134. doi:10.1016/j.molstruc.2012.02.035
24. Irfan A, Hina N, Al-Sehemi A, Asiri A (2012) J Mol Model 18:4199–4207. doi:10.1007/s00894-012-1421-4
25. Al-Sehemi A, Irfan A, Asiri A (2012) Theor Chem Acc 131:1–10. doi:10.1007/s00214-012-1199-6
26. Irfan A, Al-Sehemi A (2012) J Mol Model 18:4893–4900. doi:10.1007/s00894-012-1488-y
27. Irfan A, Jin R, Al-Sehemi AG, Asiri AM (2013) Spectrochim Acta A Mol Biomol Spectrosc 110:60–66. doi:10.1016/j.saa.2013.02.045
28. Preat J, Jacquemin D, Perpète EA (2010) Environ Sci Technol 44: 5666–5671. doi:10.1021/es100920j
29. Liu D, Fessenden RW, Hug GL, Kamat PV (1997) J Phys Chem B 101:2583–2590. doi:10.1021/jp962695p
30. Burfeindt B, Hannappel T, Storck W, Willig F (1996) J Phys Chem 100:16463–16465. doi:10.1021/jp9622905
31. Sayama K, Tsukagoshi S, Hara K et al (2002) J Phys Chem B 106: 1363–1371. doi:10.1021/jp0129380
32. Sánchez-Carrera RS, Coropceanu V, da Silva Filho DA et al (2006) J Phys Chem B 110:18904–18911. doi:10.1021/jp057462p
33. Irfan A, Al-Sehemi AG, Muhammad S (2014) Synth Met 190:27–33. doi:10.1016/j.synthmet.2014.01.017
34. Irfan A, Al-Sehemi AG, Al-Assiri MS (2014) Comp Theor Chem 1031:76–82. doi:10.1016/j.comptc.2013.12.027
35. Irfan A, Al-Sehemi AG, Al-Assiri MS (2014) J Fluorine Chem 157: 52–57. doi:10.1016/j.jfluchem.2013.11.001
36. Irfan A (2014) Comp Mater Sci 81:488–492. doi:10.1016/j.commatsci.2013.09.003
37. Irfan A, Al-Sehemi AG, Al-Assiri MS (2013) J Mol Graphics Model 44:168–176. doi:10.1016/j.jmgm.2013.06.003
38. Irfan A, Al-Sehemi AG, Kalam A (2013) J Mol Struct 1049:198–204. doi:10.1016/j.molstruc.2013.06.023
39. Irfan A (2014) Optik Intern J Light Elect Optics 125:4825–4830. doi: 10.1016/j.ijleo.2014.04.050
40. Guillaumont D, Nakamura S (2000) Dyes Pigm 46:85–92. doi:10.1016/S0143-7208(00)00030-9
41. Zhang C, Liang W, Chen H, Chen Y, Wei Z, Wu Y (2008) J Mol Struct (THEOCHEM) 862:98–104. doi:10.1016/j.theochem.2008.04.035
42. Irfan A, Cui R, Zhang J, Hao L (2009) Chem Phys 364:39–45. doi: 10.1016/j.chemphys.2009.08.009
43. Al-Sehemi A, Irfan A, Asiri A (2012) Theor Chem Acc 131:1199–1208. doi:10.1007/s00214-012-1199-6
44. Al-Sehemi A, Al-Melfi M, Irfan A (2013) Struct Chem 24:499–506. doi:10.1007/s11224-012-0103-2
45. Jin R, Irfan A (2012) Comp Theor Chem 986:93–98. doi:10.1016/j.comptc.2012.02.018
46. Al-Sehemi AG, Irfan A, El-Agrody AM (2012) J Mol Struct 1018: 171–175. doi:10.1016/j.molstruc.2012.03.018
47. Irfan A, Ijaz F, Al-Sehemi A, Asiri A (2012) J Comput Electron 11: 374–384. doi:10.1007/s10825-012-0417-8
48. Preat J, Michaux C, Jacquemin D, Perpète EA (2009) J Phys Chem C 113:16821–16833. doi:10.1021/jp904946a
49. Huong VTT, Nguyen HT, Tai TB, Nguyen MT (2013) J Phys Chem C 117:10175–10184. doi:10.1021/jp401191a
50. Scalmani G, Frisch MJ, Mennucci B, Tomasi J, Cammi R, Barone V (2006) J Chem Phys 124:094107–094115
51. Matthews D, Infelta P, Grätzel M (1996) Sol Energy Mater Sol Cells 44:119–155. doi:10.1016/0927-0248(96)00036-0
52. Pourtois G, Beljonne D, Cornil J, Ratner MA, Brédas JL (2002) J Am Chem Soc 124:4436–4447. doi:10.1021/ja017150+
53. Hsu C-P (2009) Acc Chem Res 42:509–518. doi:10.1021/ar800153f
54. Marcus RA (1993) Rev Mod Phys 65:599–610
55. Hilgendorff M, Sundström V (1998) J Phys Chem B 102:10505–10514. doi:10.1021/jp982210s
56. Zhigang Shuai LW, Song C (2012) Theory of charge transport in carbon electronic materials. Springer, New York
57. Asbury J, Wang Y-Q, Hao E, Ghosh H, Lian T (2001) Res Chem Intermed 27:393–406. doi:10.1163/156856701104202255
58. Katoh R, Furube A, Yoshihara T et al (2004) J Phys Chem B 108: 4818–4822. doi:10.1021/jp031260g
59. Hagfeldt A, Graetzel M (1995) Chem Rev 95:49–68. doi:10.1021/cr00033a003
60. Barbara PF, Meyer TJ, Ratner MA (1996) J Phys Chem 100:13148–13168. doi:10.1021/jp9605663
61. De Angelis F, SFaAS (2008) Nanotechnology 19:424002–424008. doi:10.1088/0957-4484/19/42/424002
62. Preat J (2010) J Phys Chem C 114:16716–16725. doi:10.1021/jp1050035
63. Benkö G, Kallioinen J, Korppi-Tommola JEI, Yartsev AP, Sundström V (2001) J Am Chem Soc 124:489–493. doi:10.1021/ja016561n
64. Iwai S, Hara K, Murata S, Katoh R, Sugihara H, Arakawa H (2000) J Chem Phys 113:3366–3373
65. Nalwa HS (2001) Handbook of advanced electronic and photonic materials and devices. Academic, San Diego
66. Harris DC, Bertolucci MD (1998) Symmetry and spectroscopy. Dover, New York
67. Casida ME (1995) Time-dependent density functional response theories of molecules. In: Chong DP (ed) Recent advances in density functional methods, part 1. World Scientific, Singapore
68. Zhang J, Kan Y-H, Li H-B et al (2013) J Mol Model 19:1597–1604. doi:10.1007/s00894-012-1719-2
69. Irfan A, Cui R, Zhang J, Hao L (2009) Chem Phys 364:39–45
70. Robertson N (2006) Angew Chem Int Ed 45:2338–2345. doi:10.1002/anie.200503083
71. Irfan A (2013) Mater Chem Phys 142:238–247. doi:10.1016/j.matchemphys.2013.07.011
72. Zhou Y, Eck M, Veit C et al (2011) Sol Energy Mater Sol Cells 95: 1232–1237. doi:10.1016/j.solmat.2010.12.041
73. Celik D, Krueger M, Veit C et al (2012) Sol Energy Mater Sol Cells 98:433–440. doi:10.1016/j.solmat.2011.11.049
74. Al-Sehemi AG, Irfan A, Al-Melfi MAM, Al-Ghamdi AA, Shalaan E (2014) J Photochem Photobiol A Chem 292:1–9. doi:10.1016/j.jphotochem.2014.07.003
75. Al-Sehemi AG, Irfan A, Fouda AM (2013) Spectrochim Acta A Mol Biomol Spectrosc 111:223–229. doi:10.1016/j.saa.2013.04.010
76. Sang-aroon W, Saekow S, Amornkitbamrung V (2012) J Photochem Photobiol A Chem 236:35–40. doi:10.1016/j.jphotochem.2012.03.014
77. Brabec CJ, Cravino A, Meissner D et al (2001) Adv Funct Mater 11: 374–380. doi:10.1002/1616-3028(200110)11:5<374::aid-adfm374>3.0.co;2-w